Chinese Journal of Chemical Engineering 70 (2024) 82–92

Contents lists available at ScienceDirect

Chinese Journal of Chemical Engineering

journal homepage: www.elsevier.com/locate/CJChE

Full Length Article

Modeling analysis of cobalt-based Fischer-Tropsch catalyst particles

Huashuai Wu [1, 2, *], Gang Wang [2], Yong Yang [2], Yongwang Li [2]

[1] College of Chemical Engineering and Technology, Taiyuan University of Technology, Taiyuan 030024, China
[2] National Energy Research & Development Center for Coal to Liquid Fuels, Synfuels China Company, Limited, Beijing 101400, China

ARTICLE INFO

Article history:
Received 5 November 2023
Received in revised form
27 February 2024
Accepted 29 February 2024
Available online 5 April 2024

Keywords:
Fischer-Tropsch synthesis
Kinetic modeling
Vapor–liquid equilibria
Numerical simulation
Intraparticle diffusion
Particle shapes

ABSTRACT

The influences of particle size, shape, and catalyst distribution on the reactivity and hydrocarbon product selectivity of a cobalt-based catalyst for Fischer-Tropsch synthesis were investigated in the present work. A self-consistent kinetic model for Fischer-Tropsch reaction proposed here was found to correlate experimental data well and hence was used to describe the consumption rates of reactants and formation rates of hydrocarbon products. The perturbed-chain statistical associating fluid theory equation of state was used to describe vapor–liquid equilibrium behavior associated with Fischer-Tropsch reaction. Local interaction between intraparticle diffusion and Fischer-Tropsch reaction was investigated in detail. Results showed that in order to avoid the adverse influence of intraparticle diffusional limitations on catalyst reactivity and product selectivity, the use of small particles is necessary. Large eggshell spherical particles are shown to keep the original catalyst reactivity and enhance the selectivity of heavy hydrocarbon products. The suitable layer thickness for a spherical particle with a diameter of 2 mm is nearly 0.15 mm. With the same outer diameter of 2 mm, the catalyst reactivity and heavy product selectivity of hollow cylindrical particles with a layer thickness of 0.25 mm are found to be larger than eggshell spherical particles. From the viewpoint of catalytic performance, hollow cylindrical particles are a better choice for industrial applications.

1. Introduction

The Fischer-Tropsch synthesis (FTS) is a crucial process that converts synthesis gas into liquid fuels and high value-added chemicals. The importance of intraparticle diffusion and reaction interaction behavior in FTS has long been recognized [1,2]. Elucidating reaction behavior of catalyst particles and realizing the effect of transport and reaction factors on catalyst performance is crucial for catalyst design and reactor scale-up.

In order to analyze the interaction between intraparticle diffusion and FTS reaction, a number of modeling studies have been carried out. Most of the studies employed either a simplified kinetics or Langmuir-Hinshelwood (LH) type of kinetics to calculate the consumption rate of CO, and product selectivity inside the particles was not considered [2–5]. A catalyst particle model was developed by Mandić *et al.* [6] to investigate the influence of particle shapes and process conditions on catalyst performance. In the numerical simulations, consumption rate of CO as well as formation rate of CH_4 was embedded into the catalyst particle model and the catalyst effectiveness factor η was shown to have a maximum value with the increasing of Thiele modulus Φ and could even reach values larger than 1.0.

Iglesia *et al.* [7] introduced selectivity aspects into numerical simulations. LH kinetics was utilized to describe consumption rate of CO and formation rate of CH_4. An additional model which was based on the diffusion-enhanced 1-olefin readsorption concept was used for modeling hydrocarbon product selectivity. One issue is that the empirical equation which describes a strong influence of chain length on diffusivity for 1-olefins and *n*-paraffins, $D_n \propto e^{-0.3n}$, was not confirmed experimentally. Similarly, Vervloet *et al.* [8] combined LH rate expressions of CO consumption as reported by Yates and Satterfield [9] and a chain growth parameter (α) which depends on temperature and H_2/CO ratio to model a single cobalt-based catalyst particle. It should be pointed out that the kinetic parameters used for CO consumption [9] and the expression for α [10] were obtained from experimental data with two different catalysts, respectively. In addition, the selectivity of hydrocarbon products was calculated directly according to the ideal Anderson-Schulz-Flory (ASF) plot. However, it is well-known that FTS

* Corresponding author. Tel.: +86 0351 6010111; Fax: +86 0351 6010111.
E-mail address: wuhuashuai@tyut.edu.cn (H. Wu).

https://doi.org/10.1016/j.cjche.2024.02.010
1004-9541/

product distribution actually deviates from the ideal ASF plot. Thus, values of product selectivity predicted by using ASF plot would not be very accurate.

Local interaction between intraparticle diffusion and FTS reaction was reported to depend greatly on the kinetic parameters used for rate equations and one needs to use kinetic parameters obtained from experimental data with the same catalyst [6]. A comprehensive FTS kinetic model in which both reactants consumption and hydrocarbon product selectivity were unified was utilized by Wang *et al.* [11] to model a single spherical catalyst particle. This kinetic model was developed from experimental data with an iron-based FTS catalyst [12] and selectivity of the entire products not only CH_4 selectivity were considered in the particle model. By using the same kinetic model proposed by Wang *et al.* [12], Nanduri and Mills [13] further investigated the influence of six different particle shapes and four different multicomponent flux models [14–17] on the catalyst performance. These results provided more detailed information about interactions between intraparticle diffusion and FTS reaction. It should be noted that due to lack of considering transport-enhanced effect on 1-olefin readsorption and secondary reactions (ORSR), the selectivity of hydrocarbon products predicted by the kinetic model developed by Wang *et al.* [12], however, was not that accurate.

In general, in order to describe the intraparticle diffusion and reaction behavior and its effects on catalyst reactivity and product selectivity, it is crucial to develop a catalyst particle model in which a self-consistent FTS kinetic model is embedded. The study of detailed FTS kinetics has received substantial attention and many efforts have been made on the rate expressions which are able to describe accurately FTS product distribution [18–24]. However, there is still no consensus on the rate expressions and one or more empirical parameters were often incorporated into the rate equations to describe the FTS product distribution. A detailed FTS kinetic model which is able to describe the deviation in product distribution from ASF plot and the variation of 1-olefin to *n*-paraffin (O/P) ratio with carbon number will be worth further investigating.

Therefore, the main goal of this work is to establish a particle model for a cobalt-based FTS catalyst, into which a detailed kinetics was embedded. Perturbed-chain statistical associating fluid theory (PC-SAFT) equation of state (EOS) was used to perform vapor-liquid equilibria (VLE) calculations. The detailed kinetic model considers the enhancement of VLE effect on ORSR and kinetic parameters were determined from experiment data [24–26] with an active Co/Re/γ-Al_2O_3 catalyst. The interactions between intraparticle diffusion and FTS reaction were theoretically analyzed using this multicomponent diffusion-reaction particle model. The influence of particle size, shape, and catalyst distribution on the reactivity and hydrocarbon selectivity of this cobalt-based catalyst was investigated. Simulation results are helpful in providing guidance for catalyst design.

2. Experimental

The experiments were carried out with a 25%Co/0.48%Re/γ-Al_2O_3 catalyst in a stirred tank slurry reactor and the details on catalyst preparation and experimental procedures can be found elsewhere [24,25]. It is worth noting that for the sake of minimizing physical transport resistances to ensure intrinsic kinetics data, catalyst particles with diameters of 44–90 μm and an impeller speed of 750 $r \cdot min^{-1}$ were selected. In total, 24 sets of experimental data with temperatures ranging from 478 to 503 K, pressure from 1.5 to 2.5 MPa, H_2/CO ratios from 1.4 to 2.1, and space velocity from 1.0 to 22.5 $NL \cdot g^{-1} \cdot h^{-1}$ were used to estimate kinetic parameters [24–26].

3. Modeling Methodology

3.1. Reactor model

The reactor model for a stirred tank slurry reactor was modeled as a CSTR model based on the following assumptions: (1) FTS reaction only takes place in the liquid phase; (2) VLE is achieved in this lab-scale reactor; (3) reactor is in isothermal and isobaric operation; and (4) external mass and heat transfer limitations are negligible:

$$F_{i,0} - F_i + w_{\text{cat}} \sum_{j=1}^{\text{NR}} \alpha_{ij} R_j = 0, i = 1, 2, \cdots, \text{NC} \tag{1}$$

where $F_{i,0}$ and F_i are the molar flow rates of component i at the inlet and outlet of the reactor, $mol \cdot s^{-1}$; w_{cat} is the mass of catalyst, kg; NC and NR are the total number of components and reactions, respectively; R_j is the rate of reaction j, $mol \cdot kg^{-1} \cdot s^{-1}$; α_{ij} is the stoichiometric coefficient for the ith component in reaction j. A total number of 50 *n*-paraffins (C_1 to C_{50}) and 49 1-olefins (C_2 to C_{50}) and three components (H_2, CO, and H_2O) are considered in the FTS reaction network. The corresponding matrix of the stoichiometric coefficients according to FTS reaction, α_{ij}, is presented in Table 1.

In order to obtain liquid concentrations of 1-olefins, PC-SAFT EOS was used to perform VLE calculations in the present work and parameters for the involved components, including the pure component and binary interaction parameters, have been completely parametrized and validated elsewhere [27–29]:

$$z_i = F_i \Big/ \sum_{i=1}^{\text{NC}} F_i, i = 1, 2, \cdots, \text{NC} \tag{2}$$

$$z_i = \varphi x_i + (1 - \varphi) y_i, i = 1, 2, \cdots, \text{NC} \tag{3}$$

$$x_i = K_{\text{eq},i} y_i, i = 1, 2, \cdots, \text{NC} \tag{4}$$

$$\sum_{i=1}^{\text{NC}} y_i = 1 \tag{5}$$

$$P_i = P y_i, i = 1, 2, \cdots, \text{NC} \tag{6}$$

where z_i is the molar fraction of component i at the outlet of the reactor; x_i and y_i are the molar fractions of component i in the liquid and vapor phases, respectively; φ is the total fraction of liquid phase ($0 \le \varphi \le 1$); $K_{\text{eq},i}$ is the VLE constant of component i; P is the total pressure, MPa and P_i is the partial pressure of component i, MPa.

3.2. Catalyst particle model

Fig. 1 illustrates the catalyst particles investigated in this work, namely spherical particle, eggshell spherical particle, solid cylindrical particle, hollow cylindrical particle, and thin plate particle. Catalyst particle pores are assumed to be filled with liquid wax in which reactants and products are dissolved. Fick's law is used here to describe the diffusion of components inside the particle. It is also assumed that external transport resistances are negligible and steady state condition is achieved. The mass conservation equation for component i inside a single catalyst particle could hence be expressed as follows:

Table 1
Stoichiometric coefficients matrix for FTS reaction

Species	Reactions					
	$CO+3H_2$	$2CO+4H_2$	$2CO+5H_2$	…(Reactant)…	$nCO+2nH_2$	$nCO+(2n+1)H_2$
	CH_4+H_2O	$C_2H_4+2H_2O$	$C_2H_6+2H_2O$	…(Product)…	$C_nH_{2n}+nH_2O$	$C_nH_{2n+2}+nH_2O$
CO	−1	−2	−2		$-n$	$-n$
H_2	−3	−4	−5		$-2n$	$-(2n+1)$
H_2O	1	2	2		n	n
CH_4	1	0	0		0	0
C_2H_4	0	1	0		0	0
C_2H_6	0	0	1		0	0
⋮	⋮	⋮	⋮		⋮	⋮
C_nH_{2n}	0	0	0		1	0
C_nH_{2n+2}	0	0	0		0	1

$$\frac{D_{\mathrm{eff},i}}{L_g^2}\frac{1}{\xi^n}\frac{\mathrm{d}}{\mathrm{d}\xi}\left(\xi^n\frac{\mathrm{d}c_{\mathrm{pore},i}(\xi)}{\mathrm{d}\xi}\right)+\rho_{\mathrm{P}}\sum_{j=1}^{\mathrm{NR}}\alpha_{ij}R_{\mathrm{pore},j}(\xi)=0,\quad i=1,2,\cdots,\mathrm{NC},\xi\in(0,1) \tag{7}$$

where ξ is the dimensionless distance; superscript n represents geometry (n = 2, 1, and 0 for sphere, cylinder, and thin plate, respectively); $c_{\mathrm{pore},i}$ is molar concentration of component i in the particle pores, $\mathrm{mol\cdot m^{-3}}$; ρ_{p} is catalyst particle density, $\mathrm{kg\cdot m^{-3}}$; $R_{\mathrm{pore},j}$ is jth reaction rate inside particle pores, $\mathrm{mol\cdot kg\cdot s^{-1}}$; $D_{\mathrm{eff},i}$ is the effective diffusivity of component i, $\mathrm{m^2\cdot s^{-1}}$; and L_g is geometric characteristic length, m.

Boundary conditions for different catalyst particle shapes are listed in Table 2.

The effective diffusivity of component i, $D_{\mathrm{eff},i}$, in the particle pores is calculated from:

$$D_{\mathrm{eff},i}=\frac{\varepsilon D_i}{\tau} \tag{8}$$

where D_i is the molecular diffusivity of component i in FTS wax, ε is the porosity and τ is the tortuosity factor. The molecular diffusivities of CO and H_2 in FTS wax are calculated using the following correlations [11]:

$$D_{\mathrm{CO}}=5.584\times10^{-7}\exp(-1786.29/T) \tag{9}$$

$$D_{\mathrm{H_2}}=1.085\times10^{-6}\exp(-1624.63/T) \tag{10}$$

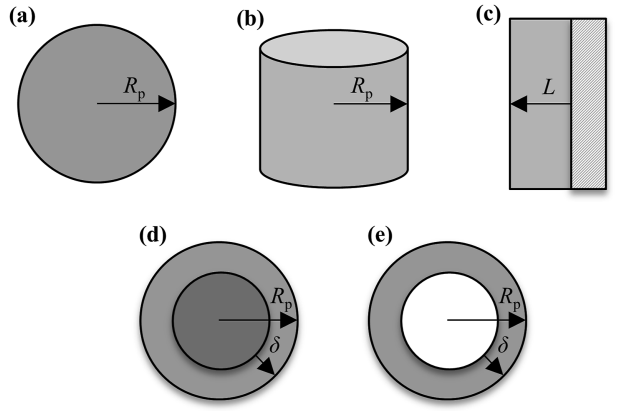

Fig. 1. Schematic representation of the particle shapes: (a) spherical particle, (b) solid cylindrical particle, (c) thin plate particle, (d) eggshell spherical particle, and (e) hollow cylindrical particle.

The molecular diffusivities of the other relevant components in FTS wax are estimated according to the correlations obtained by Erkey *et al.* [30,31]. Liquid concentration of component i, $c_{\mathrm{s,L},i}$, and total liquid concentration, $c_{\mathrm{s,L,total}}$, at the surface of catalyst particles are calculated as follows:

$$c_{\mathrm{s,L},i}=c_{\mathrm{s,L,total}}x_i \tag{11}$$

$$c_{\mathrm{s,L,total}}=\frac{\rho_{\mathrm{L}}}{M_{\mathrm{L}}} \tag{12}$$

where ρ_{L} is the liquid density, $\mathrm{kg\cdot m^{-3}}$ and M_{L} is the number-average molecular weight of wax, $\mathrm{kg\cdot mol^{-1}}$. The average density of FTS products in the liquid phase is obtained according to the correlation proposed by Marano and Holder [32] and FTS wax is approximately treated as n-octacosane [11].

The average reaction rate of ith reaction, R_j, is obtained by integration of local reaction rate, $R_{\mathrm{pore},j}$, expressed as follows:

$$R_j=\frac{\int_0^1\sum_{j=1}^{\mathrm{NR}}\alpha_{ij}R_{\mathrm{pore},j}(c_{\mathrm{pore},i},\xi)\xi^n\mathrm{d}\xi}{\int_0^1\xi^n\mathrm{d}\xi} \tag{13}$$

According to the present work, the value of the catalyst effectiveness factor on the basis of CO is the largest among all the components (including both reactants and products). Therefore, the catalyst effectiveness factor on the basis of CO, η_{CO}, is used as the indicator of catalyst reactivity, which is defined as the ratio of average reaction rate in the particle pores to the reaction rate at the surface of the particle:

$$\eta_{\mathrm{CO}}=\frac{\int_0^1\sum_{j=1}^{\mathrm{NR}}\alpha_{\mathrm{CO},j}R_{\mathrm{pore},j}(c_{\mathrm{pore,CO}},\xi)\xi^n\mathrm{d}\xi}{\int_0^1\sum_{j=1}^{\mathrm{NR}}\alpha_{\mathrm{CO},j}R_{\mathrm{pore},j}(c_{\mathrm{pore,CO}},\xi=1)\xi^n\mathrm{d}\xi} \tag{14}$$

where $R_{\mathrm{pore},j}(c_{\mathrm{pore,CO}},\xi)$ is local reaction rate of CO inside the particle and $R_{\mathrm{pore},j}(c_{\mathrm{pore,CO}},\xi=1)$ is the reaction rate of CO at the surface of the particle.

The dimensionless Thiele modulus, Φ_{CO}, is defined as below:

$$\Phi_{\mathrm{CO}}=L_{\mathrm{c}}\sqrt{\frac{\rho_{\mathrm{p}}\cdot(-R_{\mathrm{CO,s}})}{D_{\mathrm{pore},i}c_{\mathrm{CO,s}}}} \tag{15}$$

where $R_{\mathrm{CO,s}}$ is the consumption rate of CO at the catalyst surface, $\mathrm{mol\cdot kg^{-1}\cdot s^{-1}}$, $c_{\mathrm{CO,s}}$ is the concentration of CO at the catalyst surface

Table 2
Boundary conditions and characteristic length for different catalyst particle shapes

Particle shape	Boundary conditions		Characteristic geometric length L_g	Characteristic diffusion length L_c
Spherical	At $\xi = 0$, $\frac{dc_{pore,i}}{d\xi} = 0$	At $\xi = 1$, $c_{pore,i} = c_{s,L,i}$	R_p	$R_p/3$
Eggshell spherical	At $\xi = 1-\delta/R_p$, $\frac{dc_{pore,i}}{d\xi} = 0$		R_p	$R_p/3[1-(1-\delta/R_p)^3]$
Solid cylindrical	At $\xi = 0$, $\frac{dc_{pore,i}}{d\xi} = 0$		R_p	$R_p/2$
Hollow cylindrical	At $\xi = 1-\delta/R_p$, $c_{pore,i} = c_{s,L,i}$		R_p	$\delta/2$
Thin plate	At $\xi = 0$, $\frac{dc_{pore,i}}{d\xi} = 0$		L	L

in the liquid phase, mol·m^{-3}, and L_c is the characteristic diffusion length of catalyst particle, m. The characteristic geometric length L_g and characteristic diffusion length L_c of the catalyst particle are listed in Table 2, respectively.

3.3. Reaction rates

3.3.1. FTS reaction mechanism

Several possible mechanisms have been proposed for FTS reaction, including surface carbide [33,34], CO-insertion [35], and enolic [36] mechanism. However, the exact mechanism is still a matter of debate. Among the above-mentioned mechanisms, surface carbide and CO-insertion mechanisms attract the most concern and hence are adopted in this study. In total, three different interpretations of surface carbide mechanism and one interpretation of CO-insertion mechanism are proposed (designated FTS-I to FTS-IV). The major difference between these four kinetic models lies in the chain propagation step. The detailed elementary reaction steps for the derivation of different kinetic models are listed in Table S1 in the Supplementary material.

3.3.2. Derivation of rate equations

The Langmuir-Hinshelwood-Hougen-Watson (LHHW) approach applied here to derive the rate equations of FTS kinetic models has been well established by Lox and Froment [18,19] and our group [12,21,22]. The derivation is mainly based on the following assumptions: (1) elementary steps for monomer formation, chain propagation, and formation of *n*-paraffins and 1-olefins are considered to be rate-determining steps (RDSs) and others are assumed to be quasi-equilibrated; (2) rate constants of chain propagation are independent of carbon number; (3) rate constants of chain termination to form *n*-paraffins are independent of carbon number except for methane and ethane; (4) rate constants of chain termination to form 1-olefins are independent of carbon number; (5) the olefin readsorption and secondary reactions are included and the rate constants for the readsorption of 1-olefins are independent of carbon number except for ethylene.

The final rate equations of kinetic model FTS-II are shown here as an example and the detailed derivation process can be found in the Supporting Information. Rate equations for the formation of methane, ethane, ethylene, *n*-paraffins, and 1-olefins are given as follows:

$$R_{CH_4} = k_{5M} K_2 P_{H_2} \alpha_1 [s]^2 \tag{16}$$

$$R_{C_2H_6} = k_{5E} K_2 P_{H_2} \alpha_1 \alpha_2 [s]^2 \tag{17}$$

$$R_{C_nH_{2n+2}} = k_5 K_2 P_{H_2} \alpha_1 \alpha_2 \prod_{i=3}^{n} \alpha_i [s]^2, n \geq 3 \tag{18}$$

$$R_{C_2H_4} = \sqrt{K_2 P_{H_2}} (k_6 \alpha_2 \alpha_1 - k_{6E}^- x_{C_2H_4}) [s] \tag{19}$$

$$R_{C_nH_{2n}} = \sqrt{K_2 P_{H_2}} \left(k_6 \alpha_1 \alpha_2 \prod_{i=3}^{n} \alpha_i - k_6^- x_{C_nH_{2n}} \right) [s], n \geq 3 \tag{20}$$

where [C_nH_{2n+1}-s] and [H-s] are the surface fractions of adsorbed species C_nH_{2n+1}-s and H-s, respectively; $x_{C_nH_{2n}}$ is the liquid fraction of 1-olefin with carbon number *n*.

The consumption rates of CO and H_2 as well as the formation rate of H_2O are determined from the formation rates of *n*-paraffins and 1-olefins, expressed as follows:

$$R_{H_2} = -\sum_{n=1}^{50} (2n+1) R_{C_nH_{2n+2}} - \sum_{n=2}^{50} 2n R_{C_nH_{2n}} \tag{21}$$

$$R_{CO} = -\sum_{n=1}^{50} n R_{C_nH_{2n+2}} - \sum_{n=2}^{50} n R_{C_nH_{2n}} \tag{22}$$

$$R_{H_2O} = \sum_{n=1}^{50} n R_{C_nH_{2n+2}} + \sum_{n=2}^{50} n R_{C_nH_{2n}} \tag{23}$$

The fraction of vacant sites, [s], is calculated as follows:

$$[s] = \frac{1}{1 + K_1 \frac{P_{H_2}^2 P_{CO}}{P_{H_2O}} + K_2^{0.5} P_{H_2}^{0.5} + \frac{k_3 K_1 K_2^{0.5} \frac{P_{H_2}^{2.5} P_{CO}}{P_{H_2O}}}{k_4 K_1 \frac{P_{H_2}^2 P_{CO}}{P_{H_2O}} + k_{5,1} K_2^{0.5} P_{H_2}^{0.5}}} \left(1 + \sum_{i=2}^{n} \prod_{j=2}^{i} \alpha_j \right) \tag{24}$$

The chain growth probability factor for a molecule with *n* carbon atoms α_n is calculated as follows:

$$\alpha_1 = \frac{[CH_3\text{-s}]}{[H\text{-s}]} = \frac{k_3 [CH_2\text{-s}]}{k_{5M} [H\text{-s}] + k_4 [CH_2\text{-s}]} \tag{25}$$

$$\alpha_2 = \frac{[C_2H_5\text{-s}]}{[CH_3\text{-s}]} = \frac{k_4 [CH_2\text{-s}]}{k_{5E} [H\text{-s}] + k_4 [CH_2\text{-s}] + k_6 (1 - \beta_2)} \tag{26}$$

$$\alpha_n = \frac{[C_nH_{2n+1}\text{-s}]}{[C_{n-1}H_{2n-1}\text{-s}]}, n \geq 3 \tag{27}$$

Eqs. (16)–(23) combined with the equations for chain growth probabilities and concentration of 1-olefins in the liquid phase represent equations of kinetic model FTS-II.

3.4. Parameter estimation methodology

The parameters of FTS kinetic models consist of rate constants, k_i, and equilibrium constants, K_i. The dependence of rate constants k_i on temperature is evaluated using the Arrhenius-type equation:

$$k_i(T) = A_i \exp(-E_i / R_{gas}T) \tag{28}$$

where A_i is the pre-exponential factor, E_i is the activation energy, $kJ \cdot mol^{-1}$, and R_{gas} is the universal gas constant, $J \cdot mol^{-1} \cdot K^{-1}$.

To estimate the model parameters, 36 responses in the regression procedure were selected, namely, CO conversion, H_2/CO outlet ratio, individual selectivity toward CH_4, C_2, C_3, C_4, and C_{5+}, chain growth factor of C_1–C_{15} as well as individual O/P ratio of C_2–C_{15}. The objection function, F_{obj}, which should be minimized for the estimation of kinetic parameters, is expressed as follows:

$$F_{obj} = \sum_{i=1}^{N_{exp}} \sum_{j=1}^{N_{res}} w_j \left(\frac{\Omega_{ij}^{exp} - \Omega_{ij}^{cal}}{\Omega_{ij}^{exp}} \right)^2 \tag{29}$$

where Ω_{ij}^{exp} and Ω_{ij}^{cal} are the experimental and calculated values for response j in the ith experimental run, respectively; w_j is the weighting factor of quantity j; N_{res} is the number of responses and N_{exp} is the number of experimental runs.

The mean absolute relative residual (MARR) between experimental data and calculated values is used to reveal the deviations between calculated results and experimental data, expressed as:

$$MARR = \frac{1}{N_{exp}N_{res}} \times \sum_{i=1}^{N_{exp}} \sum_{j=1}^{N_{res}} \left| \frac{\Omega_{ij}^{exp} - \Omega_{ij}^{cal}}{\Omega_{ij}^{exp}} \right| \times 100\% \tag{30}$$

The values of kinetic parameters were estimated by multivariable nonlinear regression. The values of activation energies, rate constants, and equilibrium constants are confined to be in the appropriate ranges in order to obtain meaningful parameter values. The statistical tests (*F*-test and *t*-test) were used to evaluate the significance of kinetic models.

4. Results and Discussion

4.1. Quality of model predictions and estimated parameters

The foregoing proposed four kinetic models were fitted to the cobalt-based FTS kinetics data by minimizing the sum of the squares of the difference between experimental data and calculated values. MARR values for these four models, which were reported as a measure of the goodness of fit, were presented in Fig. 2. Obviously, kinetic model FTS-IV has the lowest MARR value of 15.04%. Considering the lowest MARR value, it is clear that kinetic model FTS-IV which is based on CO-insertion mechanism correlates reasonably better with experimental data than the other three proposed kinetic models.

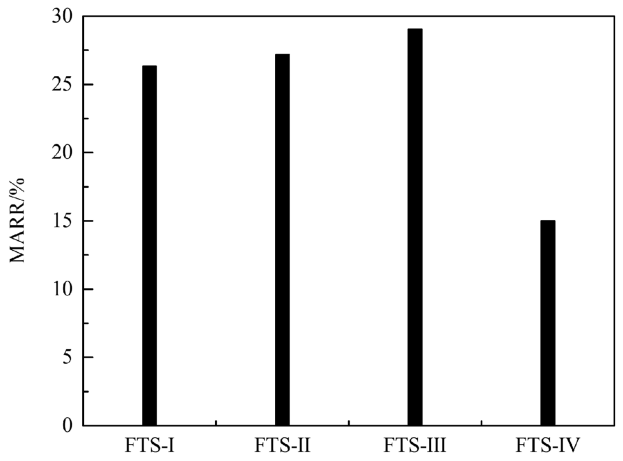

Fig. 2. MARR values between the experimental data [26] and the values calculated from FTS kinetic models.

The parameter values of the best-fitted kinetic model FTS-IV are presented in Table 3 and all of them are statistically significant. It is insightful to point out that previous kinetic models were usually at the cost of introducing empirical parameters into the rate equations to correct the formation rate or readsorption rate of 1-olefins. For the kinetic model proposed here, the empirical parameters were excluded from rate equations of 1-olefins. This means that kinetic model FTS-IV hence could be regarded as intrinsic, which represents a significant improvement in comparison to the reported kinetic models [20,22,24,25]. The activation energies for the formation of *n*-paraffins and 1-olefins, as well as methane and ethane, are within the range of the reported values. It is also noticeable that the rate constants and reaction rates of steps 6–7, which lead to the formation of *n*-paraffins and 1-olefins, were found to be at least one order of magnitude (depending on the carbon number *n* of products) slower than that of chain initiation and chain propagation steps. This indicates that product formation steps are the slowest ones in the FTS reaction process. Therefore, catalyst design should be focused on improving product formation rates. At the same time, both rate constant and formation rate of CH_4 were found to be larger than that of heavier *n*-paraffins. This fact, combined with the lowest activation energy of methane, explains a high selectivity toward CH_4. Similarly, the rate constant for ethylene readsorption is about two orders of magnitude greater than that of the other 1-olefins, which ensures a good fit of a low selectivity to ethylene.

Fit quality of kinetic model FTS-IV for CO conversion as well as CH_4 and C_{5+} selectivity is shown in Fig. 3 for all the investigated conditions. Compared with a MARR value of 23.5% obtained by Todic *et al.* [24], this represents a significant improvement in the fit quality. As shown in Fig. 4, this model accurately predicts the variation of chain growth probability and O/P ratio with carbon number in C_2–C_{15} range.

4.2. Catalyst reactivity and selectivity analysis

By using kinetic model FTS-IV, along with the same set of parameter values estimated in Section 4.1, numerical simulations with the same catalyst were performed under conditions typical of industrial practices.

4.2.1. Effect of particle size

Fig. 5 presents simulation results with spherical particles (0.1, 0.3, 1, and 2 mm, respectively). As shown in Fig. 5(a), for small particle with 0.1 mm in diameter, CO concentration decreases only slightly, and with the increasing of particle size, CO concentration profile becomes steeper and steeper. Especially, for the case of a large particle with a diameter of 2 mm, CO concentration from the point at about 0.2 mm away from the particle surface to the center of particle is very close to zero. The closer to the center of particles, the more sharply H_2/CO ratio increases. In particular, H_2/CO ratio at the center of particles becomes infinitely large for particles with diameters of 1 and 2 mm, as shown in Fig. 5(b). This in turn leads to an extremely low CO consumption rate in the interior region of catalyst particles (see Fig. 5(c)). Especially, for particles with a diameter of 1 and 2 mm, at about 0.4 and 0.2 mm away from the particle surface, CO consumption rate decreases to nearly zero. It can therefore be found that under current reaction conditions, for a

Table 3
Estimated parameter values of kinetic model FTS-IV for a cobalt-based FTS catalyst

Parameter	Value	Unit	*t*-Value①	Parameter	Value	Unit	*t*-Value①
$k_{3,ref}$	8.23×10^{-2}	$mol \cdot kg^{-1} \cdot s^{-1}$	62.78	E_7	121.74	$kJ \cdot mol^{-1}$	562.7
E_3	156.12	$kJ \cdot mol^{-1}$	274.7	k_{7E}	19.36	$mol \cdot kg^{-1} \cdot s^{-1} \cdot MPa^{-1}$	110.8
$k_{4,ref}$	7.96×10^{-2}	$mol \cdot kg^{-1} \cdot s^{-1}$	341.3	E_{7E}	164.7	$kJ \cdot mol^{-1}$	291.4
E_4	107.76	$kJ \cdot mol^{-1}$	320.3	k_7	0.23	$mol \cdot kg^{-1} \cdot s^{-1} \cdot MPa^{-1}$	13.34
$k_{6M,ref}$	4.36×10^{-2}	$mol \cdot kg^{-1} \cdot s^{-1}$	84.75	E_7	157.48	$kJ \cdot mol^{-1}$	313.0
E_{6M}	117.31	$kJ \cdot mol^{-1}$	454.9	K_1	7.64	MPa^{-1}	11.93
$k_{6E,ref}$	2.93×10^{-3}	$mol \cdot kg^{-1} \cdot s^{-1}$	182.3	K_2	4.52	MPa^{-2}	4.695
E_{6E}	134.49	$kJ \cdot mol^{-1}$	423.6	K_5	3.26	MPa^{-1}	209.6
$k_{6,ref}$	3.01×10^{-3}	$mol \cdot kg^{-1} \cdot s^{-1}$	181.4	*F*-value	232.13	–	–
E_6	136.90	$kJ \cdot mol^{-1}$	395	MARR	15.04	%	–
$k_{7,ref}$	1.27×10^{-3}	$mol \cdot kg^{-1} \cdot s^{-1}$	2272				

① *t*-Test at 95% confidence level of the reparametrized parameters. $F_{0.05}(19,864) = 1.57$, $t_{0.05} = 1.65$; $T_{ref} = 478$ K.

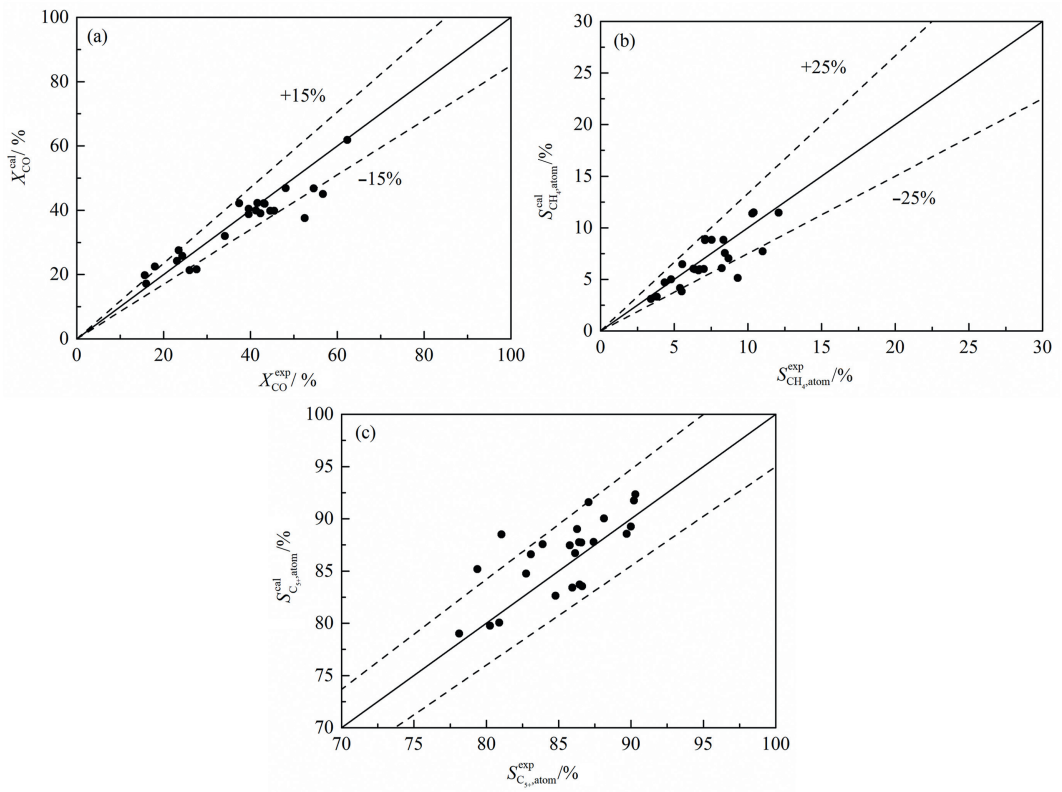

Fig. 3. Comparison of (a) CO conversion; (b) CH_4 selectivity and (c) C_{5+} selectivity calculated according to kinetic model FTS-IV to experimental data [26].

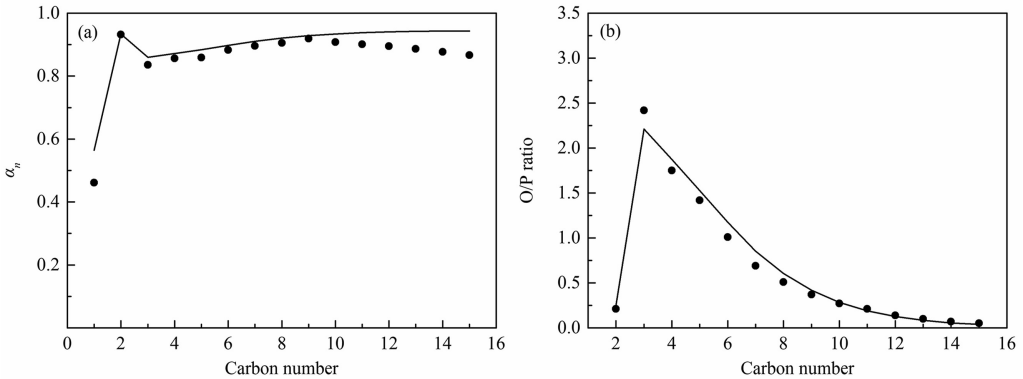

Fig. 4. Comparison of (a) chain growth probability and (b) O/P ratio predicted by kinetic model FTS-IV to experimental data [26]. Reaction conditions: $T = 478$ K, $P = 1.5$ MPa, $F = 2.1$, $SV = 2.06 \times 10^{-3}$ $m^3 \cdot kg^{-1} \cdot s^{-1}$.

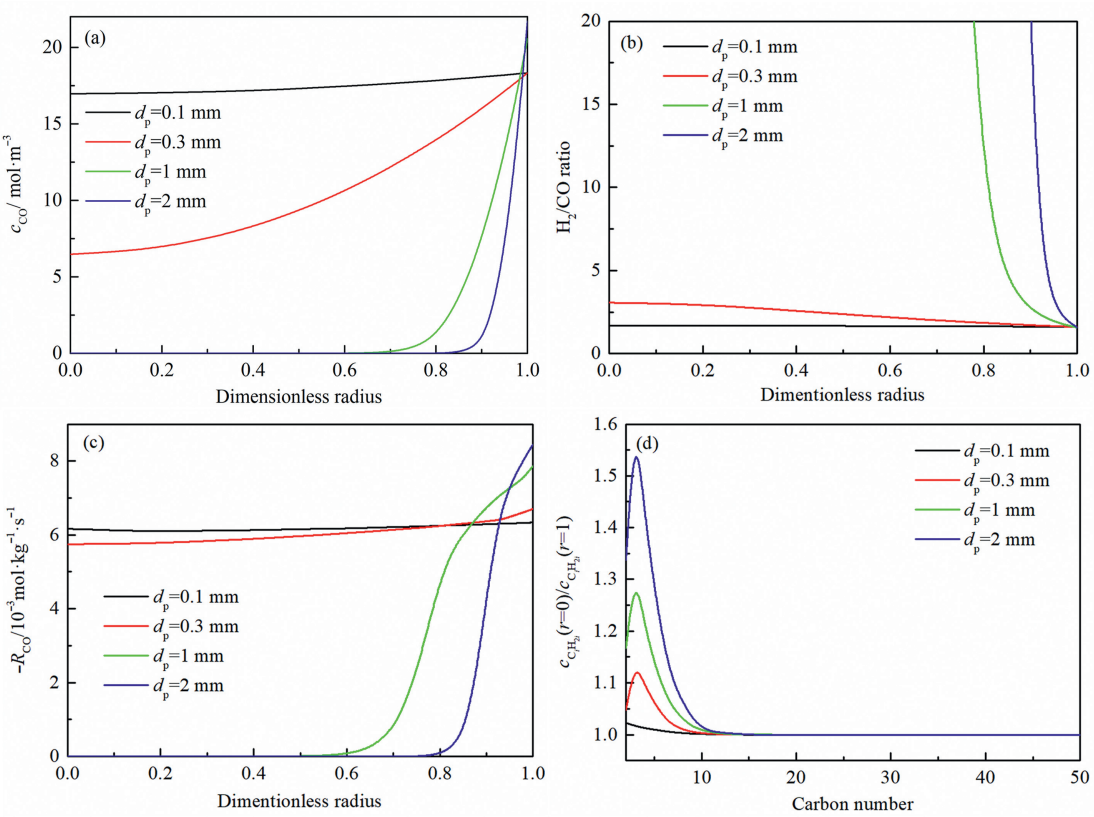

Fig. 5. (a) CO concentration profile; (b) H_2/CO ratio profile; (c) CO consumption rate profile; (d) dimensionless concentration of 1-olefins at the center of particle pore as a function of carbon number. Reaction conditions: T = 478 K, P = 1.5 MPa, F = 1.4, SV = 0.28 × 10^{-3} m^3·kg^{-1}·s^{-1}.

particle with a size of 2 mm in diameter, the effective reaction region is only located within a nearly 0.15R_p layer thickness of catalyst particle and nearly 60% of the catalysts simply do not take effect.

The concentration profiles of 1-olefins for catalyst particles with different particle sizes are presented in Fig. 5(d). With the increasing carbon number of 1-olefin, the dimensionless concentration of 1-olefin at the center of particle pores decreases and tends to be unity when the carbon number is greater than 10. This means a uniform concentration of 1-olefin with carbon number greater than 10 inside the particle pores. Therefore, compared to a lighter 1-olefin, it is, in fact, easier for a heavier 1-olefin to be transported out of the particle pores. From the above analysis, it can be seen that it is the reactant CO that has the most severe intraparticle diffusion limitations, rather than heavy 1-olefins. This suggests that minimizing the diffusion limitations of CO in the catalyst particle to some degree would be the most effective way to improve catalyst reactivity.

Fig. 6 shows the influence of particle size on catalyst effectiveness factor and reaction performance for a spherical particle. For a particle size of 0.1 mm in diameter, the value of catalyst effectiveness factor η_{CO} is close to 1.0 and in such cases, the intraparticle transport resistances could be considered to be negligible. For a spherical particle with a large diameter of 4 mm, the value of η_{CO} decreases to a relatively low value of 0.27. This corresponds to a severe diffusion limitation. The variation of CO conversion with particle size also follows the same trend as the change of η_{CO} with the increasing particle size (see Fig. 6(b)). This verifies that η_{CO} could be regarded as the catalyst reactivity indicator. As shown in

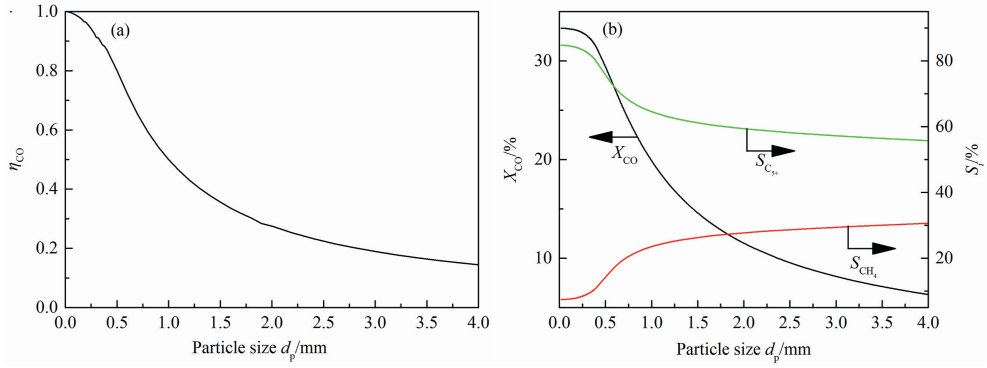

Fig. 6. (a) Catalyst effectiveness factor; (b) CO conversion, CH_4 and C_{5+} selectivity as a function of catalyst particle size. Reaction conditions: T = 478 K, P = 1.5 MPa, F = 1.4, SV = 0.28 × 10^{-3} m^3·kg^{-1}·s^{-1}.

Fig. 6(b), when particle size increases from 0.1 mm to 4 mm, CH_4 selectivity (which usually corresponds to the undesired product) increases from 7.6% to 30.6%. From Fig. 6(b), we can also see that an increase in CH_4 selectivity subsequently leads to a general decreasing trend of selectivity to C_{5+} products (which is often considered as the desired products). From the data shown in Fig. 6(b), CO conversion as well as selectivity to CH_4 and C_{5+} are almost invariant when particle size is less than 0.32 mm. In such cases, the intraparticle diffusion limitations could be considered as negligible. It is worth mentioning that small spherical particles with a diameter of 44–90 μm used in the FTS kinetics experiments are able to provide intrinsic kinetics data.

According to the foregoing analysis, it is concluded that large catalyst particles are unfavorable for the improvement of catalyst reactivity and C_{5+} selectivity owing to strong intraparticle diffusional resistance. To improve catalyst reactivity and C_{5+} selectivity, it would be better to use small particles. In realistic industrial reactors, however, an appropriate particle size should be selected, normally 2–4 mm in diameter to maintain a low-pressure drop in the fixed bed reactors [11] or not too small size to keep the wax filter working well in slurry reactors [4]. Hence, it is not feasible to just reduce the catalyst particle size to achieve better catalytic performance for industrial applications.

4.2.2. Effect of particle shape on the catalyst performance

Fig. 7 presents the change of catalyst effectiveness factor and CH_4 selectivity with Thiele modulus for three different geometric shapes (sphere, solid cylinder, and thin plate), respectively. The value of Thiele modulus, Φ_{CO}, is varied by changing particle size. As shown in Fig. 7(a), when the value of Φ_{CO} is less than 0.6, the catalyst effectiveness factor η_{CO} for all the three particle shapes is very close to 1.0. It is clear that this is the region where intraparticle diffusional limitations could be ignored. For $\Phi_{CO} > 0.6$, η_{CO} decreases to be less than 1.0 and this corresponds to the intermediate region where intraparticle diffusion comes into play. In such cases, there is a sensible difference among the Φ_{CO} *vs.* η_{CO} curves for different particle shapes. The value of η_{CO} for a spherical particle starts decreasing soonest, followed by a solid cylindrical particle, and a thin plate particle. When the value of Φ_{CO} increases to be larger than 3.0, the Φ_{CO} *vs.* η_{CO} curves for different particle shapes tend to be an identical one. This region is where intraparticle diffusional limitations predominate.

Fig. 7(b) shows that for $\Phi_{CO} < 0.6$, CH_4 selectivity for these three particle shapes nearly keeps a constant value. As the value of Φ_{CO} continues to increase, a sharp increase in CH_4 selectivity is observed. For this reason, the point at which the value of Φ_{CO} is equal to 0.6 is identified as the upper limit of the region of kinetics control. The value of η_{CO} at the upper limit of kinetics region ranges from 0.91 (sphere), 0.93 (solid cylinder), 0.94 (thin plate). This is in the same order as that is observed for the decrease in η_{CO}, that is, sphere < solid cylinder < thin plate. Therefore, for the purpose of eliminating the negative impact of intraparticle diffusion, the upper limit of the diameter of these three particles is 0.32 (sphere), 0.22 (solid cylinder), and 0.05 mm (thin plate), respectively. Obviously, the diameter of a spherical particle is the largest, followed by the solid cylindrical and thin plate particle. Hence, at the above-investigated conditions, with the same outer diameter, the use of spherical particle would be a better choice than the solid cylindrical and thin plate particles because it results in higher CO conversion, lower CH_4 selectivity, and higher C_{5+} selectivity. Also, if one wants to use this catalyst in monolith reactors at the above conditions, layer thickness of this catalyst should be less than 0.05 mm. This is in consistent with the catalyst layer thickness used in monolith reactors reported by other research groups [37,38].

For the cases of $\Phi_{CO} > 3.0$, CH_4 selectivity for different particle shapes approaches the same value with the increase in Φ_{CO}. In the intermediate region where $0.6<\Phi_{CO}< 3.0$, CH_4 selectivity for different particle shapes becomes complicated. With the increase of Φ_{CO}, we can see that for the spherical particle, the increase in CH_4 selectivity increases sooner than the other two particle shapes, following the same order as observed for decrease in η_{CO}. However, when Φ_{CO} gradually increases to a value of 1.5, the thin plate particle instead starts to increase rapidly, followed by the solid cylindrical and spherical particles. For the latter two, the aforementioned change is relatively gradual and the profiles are also close to each other.

4.2.3. Effect of catalyst distribution on the catalyst performance

It has been reported that in fixed bed reactors the use of large eggshell spherical particles is able to minimize the adverse influence of intraparticle diffusion on heavy product selectivity and also satisfy pressure drop requirements [11]. Another way is the use of hollow cylindrical particles with small layer thickness. The design goal for these two shapes is to find an optimal layer thickness to not only maintain catalyst reactivity but also enhance the selectivity to C_{5+} products and lower CH_4 selectivity.

Fig. 8 illustrates the effect of layer thickness on catalyst effectiveness factor for eggshell spherical and hollow cylindrical particles with the same outer diameter of 2 mm. In Fig. 8, as the layer thickness of these two particles decreases, the value of catalyst effectiveness factor η_{CO} increases gradually at first, and then more rapidly. When the layer thickness of these two particles decreases to an extremely small value of $0.05R_p$, the value of η_{CO} is approximately equal to 1.0. This indicates that the use of eggshell spherical

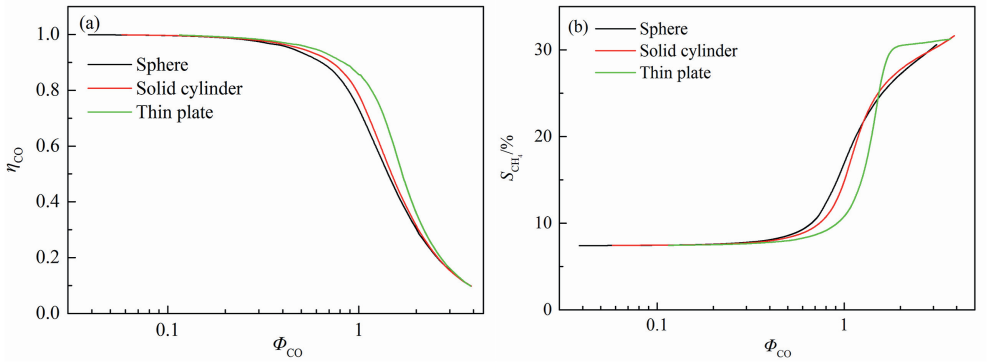

Fig. 7. (a) Catalyst effectiveness factor and (b) CH_4 selectivity as a function of Thiele modulus for different particle shapes. Reaction conditions: $T = 478$ K, $P = 1.5$ MPa, $F = 1.4$, $SV = 0.28 \times 10^{-3}$ $m^3 \cdot kg^{-1} \cdot s^{-1}$.

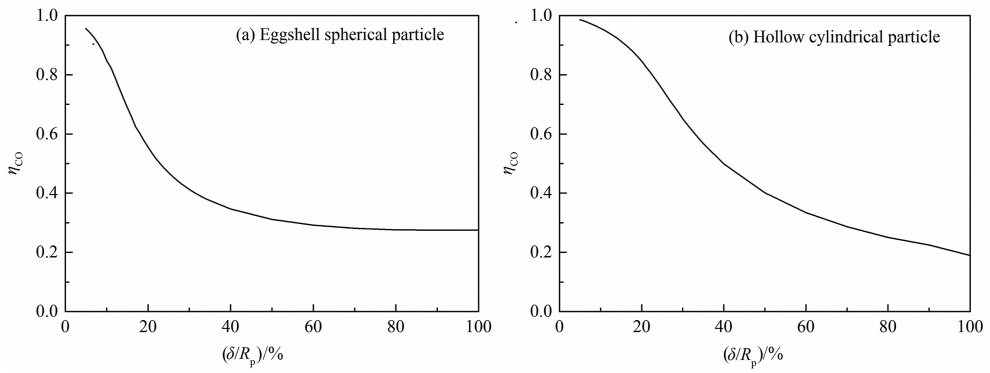

Fig. 8. Catalyst effectiveness factor as a function of layer thickness of (a) eggshell spherical particle and (b) hollow cylindrical particle. Reaction conditions: $R_p = 1$ mm, $T = 478$ K, $P = 1.50$ MPa, $F = 1.40$, SV $= 0.28 \times 10^{-3}$ $m^3 \cdot kg^{-1} \cdot s^{-1}$.

particles or hollow cylindrical particles is able to reduce the negative impact of intraparticle diffusional limitations on catalyst reactivity.

Fig. 9 shows concentration profiles of CO, H_2 and H_2O in the particle pores for four different catalyst particles with the same outer diameter of 2 mm. The layer thickness of eggshell spherical particles in Fig. 9(b) is assumed to be $0.15R_p$ while that of hollow cylindrical particles in Fig. 9(d) is assumed to be $0.25R_p$. The observed trend for hollow cylindrical particles is different from the other three particle shapes due to the fact that hollow cylindrical particles have two surfaces exposed to the surrounding fluid, while the other three have only one surface exposed to the fluid. In comparison to spherical particles and solid cylindrical particles, eggshell spherical particles and hollow cylindrical particles can avoid the extremely high H_2/CO ratio in the interior region of catalyst particles. As a result, the chain termination reactions to form light hydrocarbon products in the interior region of the catalyst particles are suppressed greatly and more heavy hydrocarbons would be produced, just as Fig. 10 shows.

Fig. 10 shows the effect of layer thickness of eggshell spherical particles and hollow cylindrical particles on CO conversion as well as selectivity to CH_4 and C_{5+} products with the same outer diameter of 2.0 mm, respectively. As Fig. 10(a) shows, when the layer thickness is greater than $0.20R_p$, CO conversion as well as CH_4 and C_{5+} selectivity are almost unchanged with the variation of layer thickness of eggshell spherical particles. When the layer thickness continuously decreases to a value of $0.15R_p$, CO conversion still remains nearly constant. At this point, CH_4 selectivity starts to

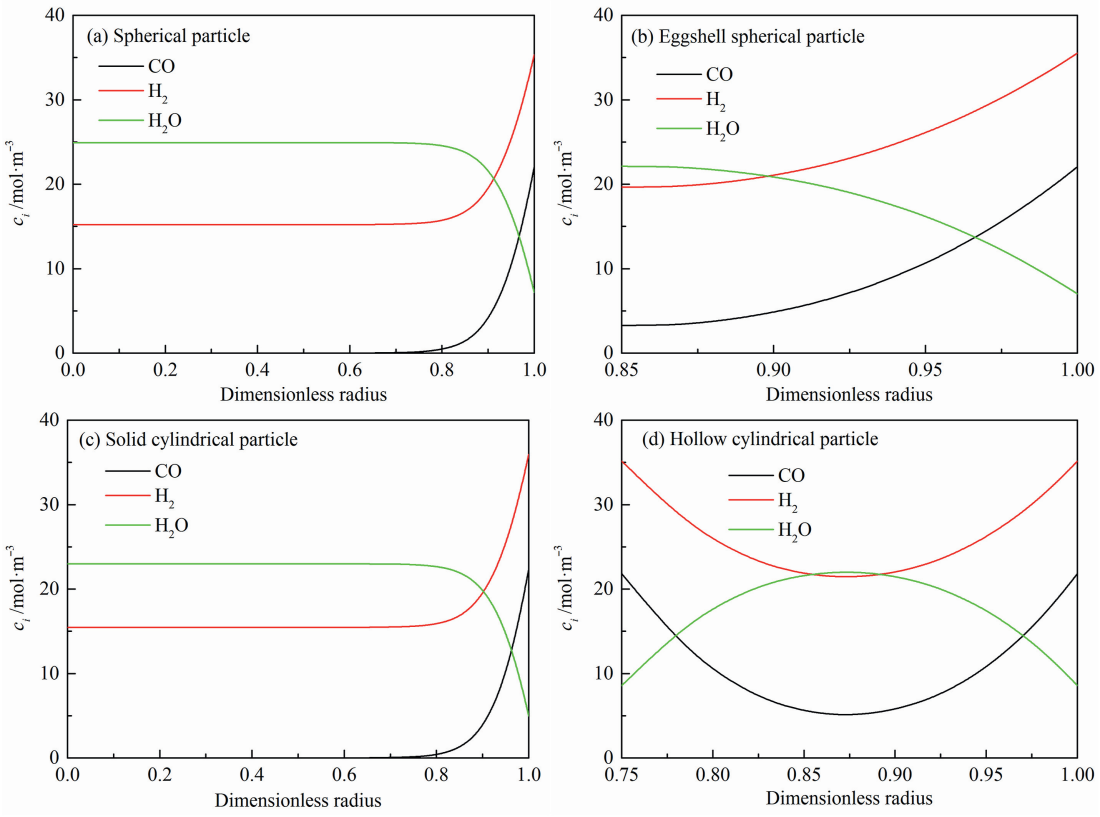

Fig. 9. Concentration profiles of CO, H_2, and H_2O for different particle shapes: (a) spherical particle, (b) eggshell spherical particle, (c) solid cylindrical particle, and (d) hollow cylindrical particle. Reaction conditions: $R_p = 1$ mm, $T = 478$ K, $P = 1.50$ MPa, $F = 1.40$, and SV $= 0.28 \times 10^{-3}$ $m^3 \cdot kg^{-1} \cdot s^{-1}$.

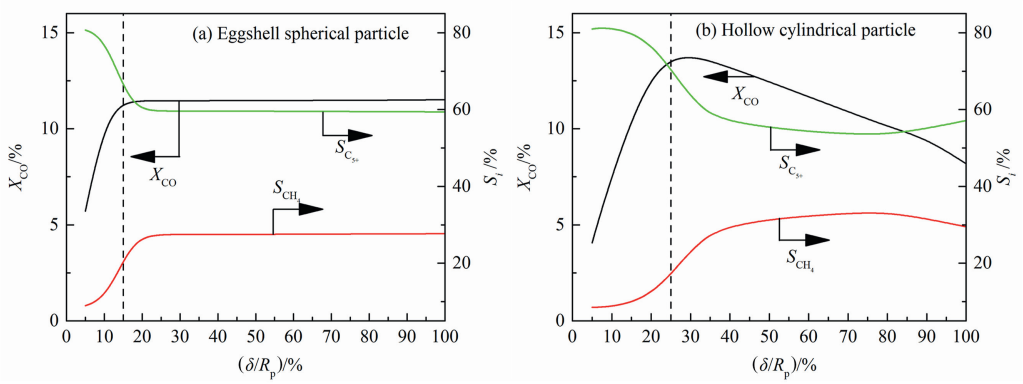

Fig. 10. CO conversion, CH_4 and C_{5+} selectivity as a function of layer thickness of (a) eggshell spherical particles and (b) hollow cylindrical particles. Reaction conditions: $R_p = 1$ mm, $T = 478$ K, $P = 1.50$ MPa, $F = 1.40$, SV $= 0.28 \times 10^{-3}$ $m^3 \cdot kg^{-1} \cdot s^{-1}$.

decrease, which subsequently leads to an increasing selectivity to C_{5+} products. In other words, although the amount of catalyst used for spherical particles with eggshell catalyst distribution is only about 40% of that used for spherical particles, the reactivity of these two particles is nearly the same. Besides, C_{5+} selectivity for eggshell spherical particles is also enhanced and CH_4 selectivity is lowered. When the layer thickness decreases to an extreme value of $0.05R_p$, CH_4 selectivity decreases rapidly and C_{5+} selectivity increases greatly, however, this is at the cost of the rapid decrease of CO conversion. This indicates that the layer thickness is very essential to not only keep the reactivity of uniform catalysts but also enhance the selectivity to C_{5+} products. Therefore, when large catalyst particles must be used, eggshell spherical particles with a moderate layer thickness will provide better performance than spherical particles.

The cases for hollow cylindrical particles are different from eggshell spherical particles. In Fig. 10(b), CO conversion passes through a maximum value of 13.5% (even larger than that for solid cylindrical particles) at approximately $0.25R_p$ with the decrease of layer thickness of hollow cylindrical particles. For hollow cylindrical particles with a layer thickness of $0.25R_p$, CH_4 selectivity is 17.3%, and this is nearly half of that for solid cylindrical particles. The selectivity towards C_{5+} products for hollow cylindrical particle is 70.4%, also higher than that for solid cylindrical particles (with a value of 57.2%). This suggests that hollow cylindrical particles with an appropriate layer thickness are also able to improve the overall catalyst reactivity and selectivity of heavy products.

From data shown in Fig. 10(a), CO conversion and selectivity towards to CH_4 and C_{5+} products for eggshell spherical particles with a layer thickness of $0.15R_p$ is 11.2%, 20.4%, and 66.6%, respectively. In comparison to eggshell spherical particles, higher catalyst reactivity was obtained with hollow cylindrical particles. This is because, with the same catalyst mass, the active sites exposed in the surface of hollow cylindrical particles are much more than that for eggshell spherical particles. As mentioned earlier, there are two surfaces exposed to the surrounding fluids for hollow cylindrical particles while only one surface is exposed to the fluids for eggshell spherical particles. This leads to a generally lower H_2/CO ratio inside the hollow cylindrical particles, thereby achieving a higher selectivity to heavy products and a lower selectivity to light products.

From the viewpoint of catalytic performance, hollow cylindrical particles with larger surface area which is exposed to the surrounding fluid were found to achieve higher catalyst reactivity and C_{5+} selectivity. However, the catalyst reactivity and mechanical strength of large hollow cylindrical particles are still low. Therefore, in order to be applied in industrial applications, special efforts are still required to be focused on the promotion of catalyst activity and the improvement of mechanical strength of catalyst particles. The present work has demonstrated a direction for the efficient design of FTS catalysts with irregular shapes.

5. Conclusions

A comprehensive catalyst particle model was established in the present work to investigate the effects of particle size, shape (sphere, solid cylinder, and thin plate), and catalyst distribution (uniform *vs.* eggshell catalyst distribution for a spherical particle, solid *vs.* hollow for a cylindrical particle) on catalyst reactivity and hydrocarbon selectivity. A self-consistent FTS kinetic model was proposed to calculate both the consumption rates of reactants and formation rates of hydrocarbon products. It was shown that the increasing chain growth probability and decreasing O/P ratio with the increasing carbon number is well predicted by considering VLE effect-enhanced 1-olefin readsorption and secondary reactions concept.

Based on this self-consistent FTS kinetic model, simulation results showed that large catalyst particles are unfavorable to improve catalyst reactivity and enhance heavy hydrocarbon selectivity. In order to avoid the adverse effect of diffusional limitations on catalyst reactivity and heavy product selectivity, spherical particles with a diameter less than 0.32 mm, or cylindrical particles with a diameter less than 0.22 mm, or thin plate particles with thickness less than 0.05 mm are preferred. Large spherical particles with eggshell catalyst distribution are shown to not only keep the original catalyst reactivity but enhance the selectivity of heavy hydrocarbon products. The suitable layer thickness for an eggshell spherical particle with a diameter of 2 mm is nearly 0.15 mm. With the increasing of layer thickness, the catalyst reactivity of hollow cylindrical particles is found to pass a maximum and even larger than that for solid cylindrical particles. With the same outer diameter of 2 mm, the catalyst reactivity of hollow cylindrical particles with a layer thickness of 0.25 mm is found to be larger than eggshell spherical particles. From the viewpoint of catalytic performance, hollow cylindrical particles with larger surface area which is exposed to the surrounding fluid were found to achieve higher catalyst reactivity and C_{5+} selectivity. The present work has demonstrated a direction for the efficient design of FTS catalysts with irregular shapes.

Declaration of Interest

The authors declare that they have no known competing financial interests or personal relationships that could have appeared to influence the work reported in this paper.

Acknowledgements

This work is supported by the National Natural Science Foundation of China (21908234), the National Key Research & Development Program of China (2020YFB0606404), the Inner Mongolia Science and Technology Agency Program (2019CG058) and Shanxi Province Natural Science Foundation (202103021223063).

Supplementary Material

Supplementary data to this article can be found online at https://doi.org/10.1016/j.cjche.2024.02.010.

References

[1] E. Iglesia, S.L. Soled, J.E. Baumgartner, S.C. Reyes, Synthesis and catalytic properties of eggshell cobalt catalysts for the Fischer-Tropsch synthesis, *Top. Catal.* 2 (1) (1995) 17–27.
[2] R.S. Dixit, L.L. Tavlarides, Integral method of analysis of Fischer-Tropsch synthesis reactions in a catalyst pellet, *Chem. Eng. Sci.* 37 (4) (1982) 539–544.
[3] W.H. Zimmerman, J.A. Rossin, D.B. Bukur, Effect of particle size on the activity of a fused iron Fischer-Tropsch catalyst, *Ind. Eng. Chem. Res.* 28 (4) (1989) 406–413.
[4] B.L. Xu, Y.N. Fan, Y. Zhang, N. Tsubaki, Pore diffusion simulation model of bimodal catalyst for Fischer-Tropsch synthesis, *AIChE J.* 51 (7) (2005) 2068–2076.
[5] B.B. Hallac, K. Keyvanloo, J.D. Hedengren, W.C. Hecker, M.D. Argyle, An optimized simulation model for iron-based Fischer–Tropsch catalyst design: Transfer limitations as functions of operating and design conditions, *Chem. Eng. J.* 263 (2015) 268–279.
[6] M. Mandić, B. Todić, L. Živanić, N. Nikačević, D.B. Bukur, Effects of catalyst activity, particle size and shape, and process conditions on catalyst effectiveness and methane selectivity for fischer–tropsch reaction: A modeling study, *Ind. Eng. Chem. Res.* 56 (10) (2017) 2733–2745.
[7] E. Iglesia, Design, synthesis, and use of cobalt-based Fischer-Tropsch synthesis catalysts, *Appl. Catal. Gen.* 161 (1–2) (1997) 59–78.
[8] D. Vervloet, F. Kapteijn, J. Nijenhuis, J.R. van Ommen, Fischer–Tropsch reaction–Diffusion in a cobalt catalyst particle: Aspects of activity and selectivity for a variable chain growth probability, *Catal. Sci. Technol.* 2 (6) (2012) 1221–1233.
[9] I.C. Yates, C.N. Satterfield, Intrinsic kinetics of the Fischer-Tropsch synthesis on a cobalt catalyst, *Energy Fuels* 5 (1) (1991) 168–173.
[10] R.M. de Deugd, Fischer–Tropsch synthesis revisited; efficiency and selectivity benefits from imposing temporal and/or spatial structure in the reactor, PhD thesis, Delft University of Technology, Delft, 2004.
[11] Y.N. Wang, Y.Y. Xu, H.W. Xiang, Y.W. Li, B.J. Zhang, Modeling of catalyst pellets for Fischer–Tropsch synthesis, *Ind. Eng. Chem. Res.* 40 (20) (2001) 4324–4335.
[12] Y.N. Wang, W.P. Ma, Y.J. Lu, J. Yang, Y.Y. Xu, H.W. Xiang, Y.W. Li, Y.L. Zhao, B.J. Zhang, Kinetics modelling of Fischer–Tropsch synthesis over an industrial Fe–Cu–K catalyst, *Fuel* 82 (2) (2003) 195–213.
[13] A. Nanduri, P.L. Mills, Effect of catalyst shape and multicomponent diffusion flux models on intraparticle transport-kinetic interactions in the gas-phase Fischer-Tropsch synthesis, *Fuel* 278 (2020) 118117.
[14] B.E. Poling, J.M. Prausnitz, J.P. O'connell, The Properties of Gases and Liquids, fifth ed., Mcgraw-Hill, New York, 2001.
[15] J. Solsvik, H.A. Jakobsen, Modeling of multicomponent mass diffusion in porous spherical pellets: Application to steam methane reforming and methanol synthesis, *Chem. Eng. Sci.* 66 (9) (2011) 1986–2000.
[16] R. Krishna, J.A. Wesselingh, The Maxwell-Stefan approach to mass transfer, *Chem. Eng. Sci.* 52 (6) (1997) 861–911.
[17] J.W. Veldsink, R.M.J. van Damme, G.F. Versteeg, W.P.M. van Swaaij, The use of the dusty-gas model for the description of mass transport with chemical reaction in porous media, *Chem. Eng. J. Biochem. Eng. J.* 57 (2) (1995) 115–125.
[18] E.S. Lox, G.F. Froment, Kinetics of the Fischer-Tropsch reaction on a precipitated promoted iron catalyst. 2. Kinetic modeling, *Ind. Eng. Chem. Res.* 32 (1) (1993) 71–82.
[19] E.S. Lox, G.F. Froment, Kinetics of the Fischer-Tropsch reaction on a precipitated promoted iron catalyst .1. Experimental procedure and results, *Ind. Eng. Chem. Res.* 32 (1) (1993) 61–70.
[20] G.P. van der Laan, A.A.C.M. Beenackers, Hydrocarbon selectivity model for the gas–solid Fischer–Tropsch synthesis on precipitated iron catalysts, *Ind. Eng. Chem. Res.* 38 (4) (1999) 1277–1290.
[21] J. Yang, Y. Liu, J. Chang, Y.N. Wang, L. Bai, Y.Y. Xu, H.W. Xiang, Y.W. Li, B. Zhong, Detailed kinetics of Fischer–Tropsch synthesis on an industrial Fe–Mn catalyst, *Ind. Eng. Chem. Res.* 42 (21) (2003) 5066–5090.
[22] B.T. Teng, J. Chang, C.H. Zhang, D.B. Cao, J. Yang, Y. Liu, X.H. Guo, H.W. Xiang, Y. W. Li, A comprehensive kinetics model of Fischer–Tropsch synthesis over an industrial Fe–Mn catalyst, *Appl. Catal. Gen.* 301 (1) (2006) 39–50.
[23] F.G. Botes, Proposal of a new product characterization model for the iron-based low-temperature Fischer–Tropsch synthesis, *Energy Fuels* 21 (3) (2007) 1379–1389.
[24] B. Todic, W.P. Ma, G. Jacobs, B.H. Davis, D.B. Bukur, CO-insertion mechanism based kinetic model of the Fischer–Tropsch synthesis reaction over re-promoted Co catalyst, *Catal. Today* 228 (2014) 32–39.
[25] B. Todic, T. Bhatelia, G.F. Froment, W.P. Ma, G. Jacobs, B.H. Davis, D.B. Bukur, Kinetic model of Fischer–Tropsch synthesis in a slurry reactor on Co–Re/Al_2O_3 catalyst, *Ind. Eng. Chem. Res.* 52 (2) (2013) 669–679.
[26] B. Todic, W.P. Ma, G. Jacobs, B.H. Davis, D.B. Bukur, Effect of process conditions on the product distribution of Fischer–Tropsch synthesis over a re-promoted cobalt-alumina catalyst using a stirred tank slurry reactor, *J. Catal.* 311 (2014) 325–338.
[27] K. Zheng, R.Y. Yang, H.S. Wu, G. Wang, Y. Yang, Y.W. Li, Application of the perturbed-chain SAFT to phase equilibria in the Fischer–Tropsch synthesis, *Ind. Eng. Chem. Res.* 58 (19) (2019) 8387–8400.
[28] K. Zheng, H.S. Wu, C.Y. Geng, G. Wang, Y. Yang, Y.W. Li, A comparative study of the perturbed-chain statistical associating fluid theory equation of state and activity coefficient models in phase equilibria calculations for mixtures containing associating and polar components, *Ind. Eng. Chem. Res.* 57 (8) (2018) 3014–3030.
[29] H.S. Wu, K. Zheng, G. Wang, Y. Yang, Y.W. Li, Modeling of gas solubility in hydrocarbons using the perturbed-chain statistical associating fluid theory equation of state, *Ind. Eng. Chem. Res.* 58 (27) (2019) 12347–12360.
[30] C. Erkey, J.B. Rodden, A. Akgerman, A correlation for predicting diffusion coefficients in alkanes, *Can. J. Chem. Eng.* 68 (4) (1990) 661–665.
[31] C. Erkey, J.B. Rodden, A. Akgerman, Diffusivities of synthesis gas and *n*-alkanes in Fischer-Tropsch wax, *Energy Fuels* 4 (3) (1990) 275–276.
[32] J.J. Marano, G.D. Holder, Prediction of bulk properties of Fischer–Tropsch derived liquids, *Ind. Eng. Chem. Res.* 36 (6) (1997) 2409–2420.
[33] F. Fischer, H. Tropsch, Die erdölsynthese bei gewöhnlichem druck aus den vergasungsprodukten der kohlen, *Brennstoff. Chem* 7 (1926) 97.
[34] R.C. Brady III, R. Pettit, Mechanism of the Fischer-Tropsch reaction. The chain propagation step, *J. Am. Chem. Soc.* 103 (5) (1981) 1287–1289.
[35] H. Pichler, H. Schulz, Neuere Erkenntnisse auf dem Gebiet der synthese von kohlenwasserstoffen aus CO und H_2, *Chem. Ing. Tech.* 42 (18) (1970) 1162–1174.
[36] R.B. Anderson, R.A. Friedel, H.H. Storch, Fischer-Tropsch reaction mechanism involving stepwise growth of carbon chain, *J. Chem. Phys.* 19 (3) (1951) 313–319.
[37] F. Kapteijn, R.M. de Deugd, J.A. Moulijn, Fischer–Tropsch synthesis using monolithic catalysts, *Catal. Today* 105 (3–4) (2005) 350–356.
[38] A.M. Hilmen, E. Bergene, O.A. Lindvåg, D. Schanke, S. Eri, A. Holmen, Fischer–Tropsch synthesis on monolithic catalysts of different materials, *Catal. Today* 69 (1–4) (2001) 227–232.